

RESEARCH ARTICLE

Estrous cycle impacts on dendritic spine plasticity in rat nucleus accumbens core and shell and caudate–putamen

 Anna L. S. Beeson^{1,2}  | John Meitzen^{1,3,4} 

¹Department of Biological Sciences, North Carolina State University, Raleigh, North Carolina, USA

²Graduate Program in Biology, North Carolina State University, Raleigh, North Carolina, USA

³Comparative Medicine Institute, North Carolina State University, Raleigh, North Carolina, USA

⁴Center for Human Health and the Environment, North Carolina State University, Raleigh, North Carolina, USA

Correspondence

John Meitzen, Department of Biological Sciences, North Carolina State University, Campus Box 7617, Raleigh, NC 27695, USA.
Email: jmeitze@ncsu.edu

Funding information

National Institute of Mental Health, Grant/Award Number: R01MH109471; National Institute of Environmental Health Sciences, Grant/Award Number: P30ES025128

Abstract

An important factor that can modulate neuron properties is sex-specific hormone fluctuations, including the human menstrual cycle and rat estrous cycle in adult females. Considering the striatal brain regions, the nucleus accumbens (NAc) core, NAc shell, and caudate–putamen (CPu), the estrous cycle has previously been shown to impact relevant behaviors and disorders, neuromodulator action, and medium spiny neuron (MSN) electrophysiology. Whether the estrous cycle impacts MSN dendritic spine attributes has not yet been examined, even though MSN spines and glutamatergic synapse properties are sensitive to exogenously applied estradiol. Thus, we hypothesized that MSN dendritic spine attributes would differ by estrous cycle phase. To test this hypothesis, brains from adult male rats and female rats in diestrus, proestrus AM, proestrus PM, and estrus were processed for Rapid Golgi–Cox staining. MSN dendritic spine density, size, and type were analyzed in the NAc core, NAc shell, and CPu. Overall spine size differed across estrous cycle phases in female NAc core and NAc shell, and spine length differed across estrous cycle phase in NAc shell and CPu. Consistent with previous work, dendritic spine density was increased in the NAc core compared to the NAc shell and CPu, independent of sex and estrous cycle. Spine attributes in all striatal regions did not differ by sex when estrous cycle was disregarded. These results indicate, for the first time, that estrous cycle phase impacts dendritic spine plasticity in striatal regions, providing a neuroanatomical avenue by which sex-specific hormone fluctuations can impact striatal function and disorders.

KEYWORDS

caudate–putamen, dendritic spine, estradiol, estrous cycle, nucleus accumbens, sex differences

1 | INTRODUCTION

Sex-specific hormone cycles occur in reproductively mature mammals, including the female rat. During the rat estrous cycle, dynamic changes in hormones including 17β -estradiol (estradiol) and progesterone occur within distinct phases over 4–5 days. These phases include diestrus (sometimes further divided into metestrus and diestrus),

proestrus AM, proestrus PM, and estrus (Adams et al., 2018; Freeman, 1994; Scharfman & MacLusky, 2006; Scharfman et al., 2007). In the 1- to 2-day diestrus phase, circulating concentrations of estradiol and progesterone begin relatively low. Estradiol then rises slowly late in diestrus. Then, estradiol levels rapidly surge on the morning of proestrus, during the proestrus AM phase. This surge in estradiol occurs over the course of hours and starts to decline in the afternoon.

This is an open access article under the terms of the [Creative Commons Attribution-NonCommercial](https://creativecommons.org/licenses/by-nc/4.0/) License, which permits use, distribution and reproduction in any medium, provided the original work is properly cited and is not used for commercial purposes.

© 2023 The Authors. *The Journal of Comparative Neurology* published by Wiley Periodicals LLC.

Later that evening, during the proestrus PM phase, progesterone concentrations peak. Thus, in rats this peak in progesterone occurs after the peak in estradiol. Following this rapid hormone fluctuation is a typical 1-day estrus in which estradiol and progesterone are low, though select effects of these hormones persist, especially in behavior and neural structures (Ajayi & Akhigbe, 2020; Hashimoto et al., 1987; Micevych & Meisel, 2017; Micevych et al., 2017). While the structure and function of organs such as the ovary, hypothalamus, and pituitary famously change between each cycle phase, other brain regions and their constituent cells are also potentially highly sensitive to this cycle. Only a few select brain regions and cell types have been assessed for sensitivity to the estrous cycle. Regarding neural anatomical structure such as dendritic spines, mammalian brain regions such as the hippocampus, prefrontal cortex, and ventromedial nucleus of the hypothalamus all show differences across estrous cycle phases (Chen et al., 2009; González-Burgos et al., 2015; Rasia-Filho et al., 2004; Woolley & McEwen, 1993). Changes in dendritic spines are particularly salient. Dendritic spines play important roles in synaptic connectivity and plasticity. Indeed, structures such as the rat hippocampus exhibit concomitant changes in neuronal synaptic electrophysiology between estrous cycle phases (Harte-Hargrove et al., 2015; Scharfman et al., 2003; Woolley et al., 1997).

These changes in electrophysiology are not limited to the hippocampus. Rat striatal brain regions also exhibit changes in physiology associated with the estrous cycle. These regions include the nucleus accumbens (NAc) core, NAc shell, and the caudate-putamen (CPU), which mediate important processes including motor control, habit formation, and reward and motivated behaviors, among many other functions (Floresco, 2015; Graybiel & Grafton, 2015). For instance, in the NAc core, the frequency and amplitude of miniature excitatory postsynaptic currents (mEPSCs) changes across the estrous cycle in the most common striatal neuron type, the medium spiny neuron (MSN) (also called spiny projection neurons) (Proaño et al., 2018, 2020). MSNs represent the output neurons of all striatal regions and exhibit dendritic spines. mEPSCs are a direct functional assessment of AMPA receptor-mediated synapses and can correlate with dendritic spine attributes (Proaño et al., 2018; Schwarz et al., 2008; Wissman et al., 2011). mEPSC frequency and amplitude correlate with circulating estradiol and progesterone concentrations, and are rapidly sensitive to acute exogenous estradiol exposure (Krentzel et al., 2019; Proaño et al., 2018, 2020). MSN dendritic spine attributes and other glutamatergic synapse-associated markers have been shown to differ by sex and exhibit plasticity in response to exogenous estradiol exposures. MSN dendritic spine density in the gonadectomized female hamster and rat decreases in response to exogenous estradiol exposure in the NAc core, and to a lesser extent, the NAc shell (Peterson et al., 2015a; Staffend et al., 2011). Exogenous estradiol acts to decrease spine density in the NAc core via an mGluR5 and endocannabinoid-mediated pathway (Gross et al., 2016; Peterson et al., 2015a). An investigation of spine dynamics in the naturally cycling animal has yet to be undertaken. This is a critical knowledge gap given the importance of dendritic spines for neuronal computation, the changes in MSN elec-

trophysiological function across the estrous cycle, and the known role of the striatal regions in mediating behaviors sensitive to estrous cycle phase.

Here, we tested the overall hypothesis that MSN dendritic spine attributes differ by estrous cycle phase. Brains from adult male rats and female rats in diestrus, proestrus AM, proestrus PM, and estrus were processed for Rapid Golgi-Cox staining to visualize MSN dendritic spines. MSN dendritic spine density, size, and type were evaluated in the NAc core, NAc shell, and CPU. We first tested the hypothesis that dendritic spine density differs between striatal regions independent of sex or the estrous cycle to replicate previous findings and validate our approach. We then disaggregated the spine data by sex to test the hypothesis that dendritic spine attributes differ by sex independent of estrous cycle phase. Next, we tested the hypothesis that spine attributes differ by estrous cycle phase within each striatal region. Finally, we examined the distribution of spine types in males and females in each estrous cycle phase for each striatal region.

2 | METHODS

2.1 | Animals

All animal protocols were approved by the Institutional Animal Care and Use Committees at North Carolina State University and Charles River Laboratories. Postnatal day 50 (P50) male and female Sprague-Dawley CD IGS rats were purchased from Charles River Laboratories (males: $n = 11$; females: $n = 33$). All animals were housed in a temperature- and light-controlled room (23°C, 40% humidity, 12:12 h light-dark cycle with lights turned on and off at 7:00 a.m. and 7:00 p.m., respectively) at the Biological Resource Facility of North Carolina State University. All cages were polysulfone bisphenol A free and were filled with bedding manufactured from virgin hardwood chips (Beta Chip; NEPCO, Warrensburg, NY) to avoid endocrine disruptors present in corncob bedding (Landeros et al., 2012; Mani et al., 2005). Soy protein-free rodent chow (2020X; Teklad, Madison, WI) and glass bottle-provided water were available ad libitum. Females were distributed across the following phases of the estrous cycle: diestrus ($n = 8$), proestrus AM ($n = 9$), proestrus PM ($n = 8$), and estrus ($n = 8$). Age (days) at sacrifice was as follows (presented as mean \pm SE): proestrus AM (77.44 ± 5.05), proestrus PM (70.63 ± 4.59), estrus (74.88 ± 5.14), diestrus (65.50 ± 1.00), and male (73.00 ± 3.92). Age of animal did not differ by group ($F(4,39) = 1.074$, $p = .3823$). Estrous cycle assessment was performed with a wet mount preparation as previously described (Hubscher et al., 2005; Proaño et al., 2018). Briefly, females were vaginally swabbed with potassium phosphate buffer solution at ~9:00 a.m. for diestrus, proestrus AM, or estrus and ~5:15 p.m. for proestrus PM. Slides were visualized under a microscope to determine estrous cycle phase according to cell morphology as previously described (Proaño et al., 2020; Westwood, 2008).

2.2 | Golgi impregnation and slide preparation

Animals were euthanized using deep anesthesia with isoflurane followed by decapitation (~9:30 a.m. or ~6:00 p.m.) and their brains rapidly removed. Golgi–Cox staining was performed on whole brains using the FD Rapid GolgiStain™ Kit (FD NeuroTechnologies, Columbia, MD). Whole brains were submerged for 1 h in ice-cold oxygenated artificial cerebrospinal fluid containing (in mM): 126 NaCl, 26 NaHCO₃, 1 MgCl₂, 1.25 NaH₂PO₄, 10 dextrose, and 2 CaCl₂, and 3 KCl from Fisher Scientific, Pittsburg, PA; osmolarity 295–305 mOsm, pH 7.2–7.4. Whole brains were then placed in a 1:1 mixture of FD Solution A:B, prepared at least 24 h in advance, for 2 weeks at room temperature in the dark. Select brains remained in Solution A:B for 11 weeks due to COVID-19-related mandated shutdowns ($n = 10$). The Golgi impregnation process that occurred while in Solution A:B did not appear adversely affected by the longer incubation time, though the tissue was more fragile during sectioning, consistent with previous observations (Rosoklija et al., 2014). Brains were then moved to FD Solution C for 72 h at room temperature in the dark. Both Solution A:B and Solution C were replaced after the first 24 h. Brains were then immersed in 30% (w/v) sucrose in distilled water for 1–10 days ($n = 36$), or 11 weeks due to COVID-19-related mandated shutdowns ($n = 8$), for cryoprotection and storage prior to sectioning. No differences between tissue stored in the sucrose mixture for 1–10 days or 11 weeks were observed in spine density, width, length, or width/length ratio ($p > .05$ for all). Tissue embedding medium (OCT Compound; Fisher HealthCare, Houston, TX) cooled by dry ice was used for affixing Golgi-impregnated whole brains to the stage of a freezing microtome (American Optical Corp., Buffalo, NY). A series of 200 μm coronal sections were collected containing the NAc core and shell, and caudate putamen (CPu) striatal regions between ~0.24 and ~5.16 from Bregma (Paxinos & Watson, 2005) onto gelatin-coated slides (FD NeuroTechnologies). Sections were allowed to dry at room temperature in the dark for at least 72 h prior to staining slides as described in the FD Rapid GolgiStain Kit. Permount™ (Fisher) was used for cover slipping.

2.3 | Imaging and spine analysis

MSNs, identified by their medium-sized, round soma and spiny dendrites (Meredith et al., 1992), were imaged between ~0.96 and ~2.04 Bregma (Paxinos & Watson, 2005) in the NAc core, NAc shell, and CPu (Figure 1). Hemispheric origin was noted to enhance equitable sampling but was not addressed as an experimental variable in this study. A series of images of Golgi-impregnated dendrites was acquired for neurons whose dendrites could be traced back to the originating soma (Figure 2). Image acquisition was conducted blind to experimental group on a Nikon Eclipse 55i microscope (Nikon, Japan) with Nikon 100 \times oil immersion objective (Fluor 100 \times /1.30 0.1 DIC H ∞ /0.17 WD 0.20) and Nikon Digital Sight DS-Fi1 camera controlled with Digital Sight Software (Nikon, Japan) using techniques



FIGURE 1 Location of analyzed medium spiny neuron (MSN) dendritic segments in adult rat nucleus accumbens (NAc) core, NAc shell, and caudate–putamen (CPu). (a) Males. (b) Females in diestrus. (c) Females in proestrus AM. (d) Females in proestrus PM. (e) Females

(Continues)

FIGURE 1 (Continued)

in estrus. Triangles represent analyzed dendritic segment location within slice. 3V, third ventricle; AC, anterior commissure; LV, lateral ventricle; NAc, nucleus accumbens; CPu, caudate-putamen.

from a previously published study (Jackson et al., 2020). Following a published protocol (Risher et al., 2014), images were coded so that analysis was also conducted blind, imported into ImageJ (ver. 1.53a, Java 8; <https://imagej.nih.gov/ij/>), converted to RGB color, and saved as separate image sequences for further analysis in RECONSTRUCT (<https://synapseweb.clm.utexas.edu/software-0>; Fiala, 2005; Risher et al., 2014). In the RECONSTRUCT software, optical section thickness was set to 0.5 microns and pixel size was adjusted to reflect microns per pixel calculated from microscope images. Dendrite and dendritic spine measurements were performed by an observer blinded to treatment groups as previously described (Risher et al., 2014). Fully impregnated dendritic segments ~10 μm in length within frame of the originating soma and free from obstruction by neighboring structures were analyzed. Analyzed dendritic segments were required to be within frame of the originating soma to ensure correct attribution of neuron type, location, and attachment to soma. The distance from the soma of the targeted dendritic segments ranged from 21 to 123 μm , encompassing both primary and secondary dendrites and excluding the aspiny soma-adjacent region previously documented in the literature (Meredith et al., 1992). One dendritic segment was analyzed per neuron, and served as the experimental unit (reported per group in Tables 1–3). Dendritic segment length was measured and all spines originating from this selected dendritic segment were measured for spine head width and spine length from dendritic trunk to spine head end in RECONSTRUCT. Both spine length and dendritic segment length measurements were performed using the “Draw Z trace” tool to trace in-focus images throughout the image series, while spine head width was measured with the “Draw line” tool for a straight, two-dimensional measurement. Intra- and intercurator controls revealed <6.5% difference between analyses of the same dendritic segment.

Data sets for each analyzed dendritic segment were constructed in Excel (Microsoft, ver. 2016 [16.0.5239.1001]). Spine attributes were calculated as following a previously published protocol (Risher et al., 2014). Spine density was calculated by dividing the total number of spines on a dendritic segment by the length of the dendritic segment (spines/ μm). Spine size was assessed by calculating the average length, width, and length:width ratio (length/width) for all individual spines on a dendritic segment. To classify spine type, spines were hierarchically and subsequently categorized using the following parameters: branched (all spines designated as “branch” during RECONSTRUCT analysis), filopodia (length > 2 μm), mushroom (width > 0.6 μm), long thin (length > 1 μm), thin (length:width ratio > 1 μm), and stubby (length:width ratio \leq 1 μm) (Figure 3) (Risher et al., 2014). Once a spine is assigned to a spine-type group, it cannot be a member of another group. Spine-type percent of total was calculated by dividing the number of a particular spine type (e.g., total

number of filopodia spines) by the total number of spines for a dendritic segment.

2.4 | Statistics

Data were analyzed with unpaired two-tailed *t*-tests using Welch's correction, one-way ANOVA with Fisher's LSD multiple comparison test, or a two-way ANOVA with Fisher's LSD multiple comparison test as appropriate (GraphPad Prism 9.0). All *p*-values of .05 were considered a priori as significant. Data values are represented as mean \pm SEM.

3 | RESULTS**3.1 | Dendritic spine density was increased in NAc core compared to NAc shell and CPu**

We first tested the hypothesis that dendritic spine density differed between striatal regions independent of sex or the estrous cycle. It has previously been shown that MSN dendritic spine density is greater in the NAc core than the NAc shell region (Bello-Medina et al., 2016; Forlano & Woolley, 2010; Meredith et al., 1992). As a control experiment to validate our approach for analyzing spine attributes, we analyzed spine density and spine size independent of sex and the estrous cycle in the NAc core (Figure 4a), NAc shell (Figure 4b), and CPu (Figure 4c). Average spine length:width ratio, indicating average spine size, did not differ by striatal region (Figure 4d) ($F(2,252) = 0.2289$, $p = .7956$). Overall, spine density differed by striatal region. Spine density, or spines/ μm , in the NAc core was significantly elevated compared to both the NAc shell and CPu (Figure 4e) ($F(2,252) = 6.249$, $p = .0022$; NAc core: 2.008 ± 0.04942 , $n = 86$; NAc shell: 1.809 ± 0.05481 , $n = 88$; CPu: 1.775 ± 0.04496 , $n = 81$). Spine density in the CPu and NAc shell did not differ from one another. These results showed that there are differences in spine density between striatal regions, replicating previous findings and validating our approach.

3.2 | No differences in spine attributes by sex, independent of estrous cycle

We next disaggregated the data by sex to test the hypothesis that dendritic spine attributes differed by sex, in this case independent of estrous cycle phase. No differences in spine size by sex were detected in the NAc core (Figure 5a), NAc shell (Figure 5b), and CPu (Figure 5c) (NAc: $t(15.87) = 1.036$, $p = .3156$, female $n = 73$, male $n = 13$; NAc shell: $t(22.10) = 1.760$, $p = .0922$, female $n = 73$, male $n = 15$; CPu: $t(17.31) = 1.042$, $p = .3117$, female $n = 65$, male $n = 16$). Likewise, no differences in spine density by sex were detected in the NAc core (Figure 5d), NAc shell (Figure 5e), or CPu (Figure 5f) (NAc core: $t(16.76) = 0.4612$, $p = .6506$; NAc shell: $t(18.94) = 0.3445$, $p = .7343$; CPu: $t(22.79) = 1.398$, $p = .1755$). Overall, no differences were detected between male and female groups when estrous cycle was not considered.

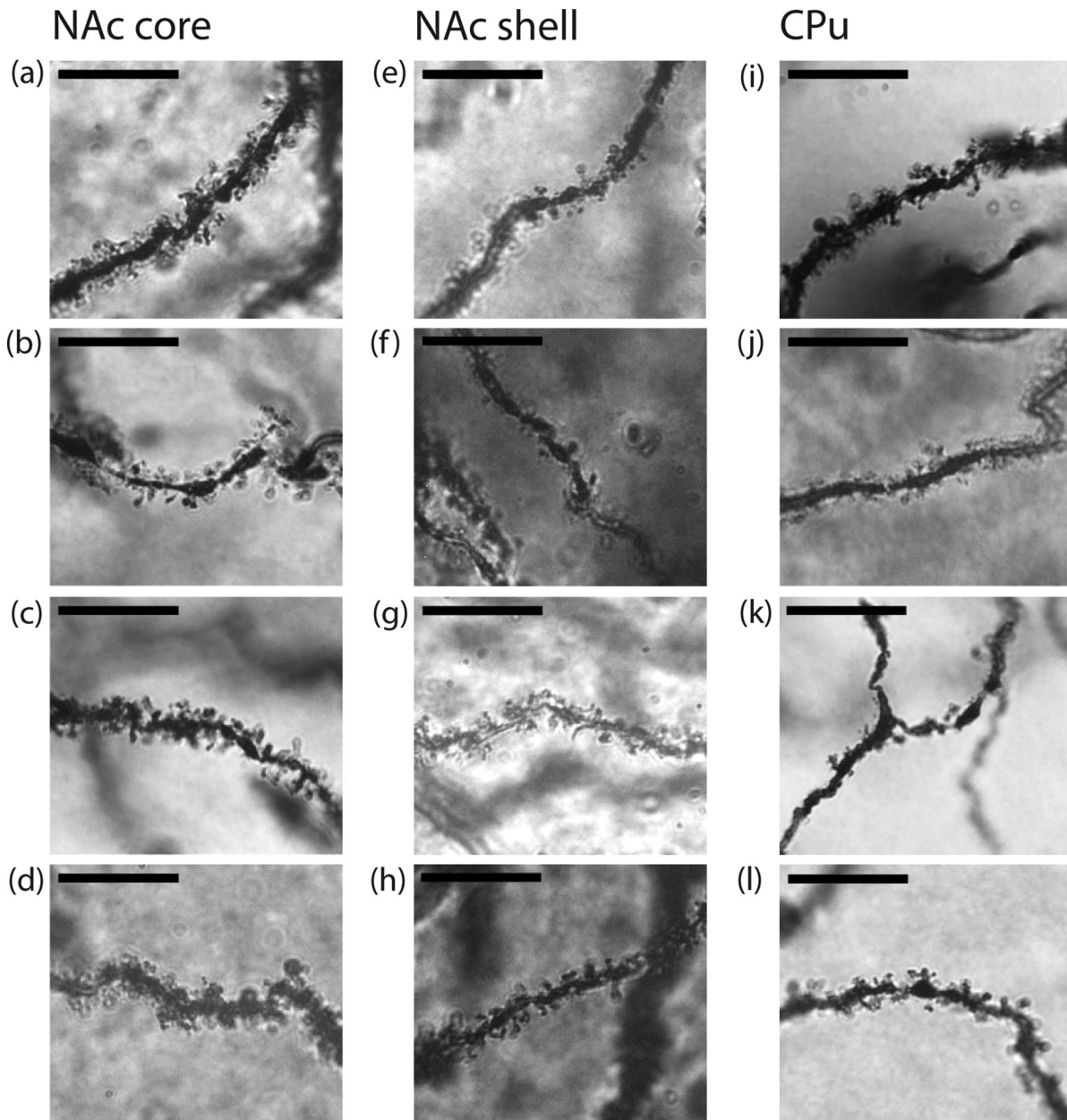


FIGURE 2 Representative images of Golgi-impregnated dendritic segments from MSNs in (a–d) NAc core, (e–h) NAc shell, and (i–l) CPu. (a) Male. (b) Female in proestrus PM. (c) Male. (d) Female in proestrus AM. (e) Female in estrus. (f) Female in diestrus. (g) Female in proestrus PM. (h) Female in diestrus. (i) Female in proestrus AM. (j) Female in diestrus. (k) Male. (l) Female in proestrus AM. Scale bar 5 μ m.

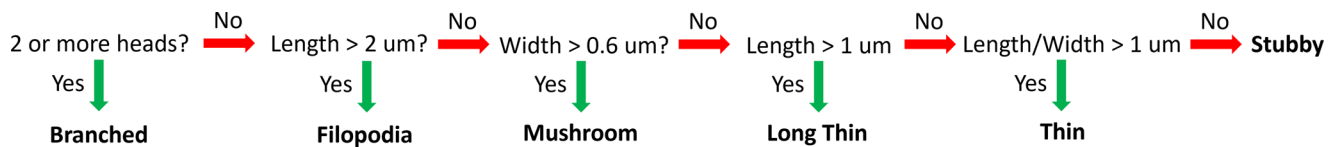


FIGURE 3 Schematic representing spine classification protocol, following Risher et al. (2014). Spine length, width, length:width ratio, and head number were first assessed. These attributes were then used to hierarchically and subsequently classify spines into the following types: branched (all spines exhibiting more than one head), filopodia (length > 2 μ m), mushroom (width > 0.6 μ m), long thin (length > 1 μ m), thin (length:width ratio > 1 μ m), and stubby (length:width ratio \leq 1 μ m).

TABLE 1 NAc core dendritic spine types for males and females across estrous cycle phases.

	Filopodia	Long Thin	Thin	Stubby	Mushroom	Branched	Statistics (<i>F</i> , <i>p</i>)
Diestrus	12.1 ± 1.9 (24) ^a	33.6 ± 2.7 (24) ^b	26.1 ± 3.0 (24) ^b	6.6 ± 1.0 (24) ^c	13.6 ± 1.9 (24) ^a	7.9 ± 1.7 (24) ^{a,c}	4.369 × 10 ⁻¹² , <.0001
Proestrus AM	19.2 ± 3.4 (15) ^{a,b}	29.5 ± 2.5 (15) ^c	25.0 ± 3.5 (15) ^{b,c}	3.9 ± 1.2 (15) ^d	13.0 ± 1.8 (15) ^a	9.3 ± 2.6 (15) ^{a,d}	4.151 × 10 ⁻¹² , <.0001
Proestrus PM	14.0 ± 2.4 (23) ^a	27.1 ± 3.3 (23) ^b	29.2 ± 3.1 (23) ^b	9.5 ± 2.2 (23) ^{a,c}	16.2 ± 2.2 (23) ^a	4.0 ± 1.3 (23) ^c	4.764 × 10 ⁻¹² , <.0001
Estrus	16.9 ± 3.2 (11) ^a	31.5 ± 3.8 (11) ^b	25.7 ± 3.6 (11) ^{a,b}	3.8 ± 1.0 (11) ^c	14.0 ± 3.0 (11) ^{a,d}	8.1 ± 2.2 (11) ^{c,d}	5.837 × 10 ⁻¹² , <.0001
Males	13.7 ± 1.5 (13) ^a	32.3 ± 3.3 (13) ^b	25.9 ± 2.8 (13) ^b	3.6 ± 1.8 (13) ^c	14.5 ± 2.2 (13) ^a	10.1 ± 2.4 (13) ^{a,c}	1.361 × 10 ⁻¹¹ , <.0001

Note: Values are spine type percent of total, mean ± SEM. Numbers in parentheses indicate number of dendritic segments analyzed. Different superscript letters indicate statistically significant differences between dendritic spine types. Spine types with the same superscript letter do not significantly differ.

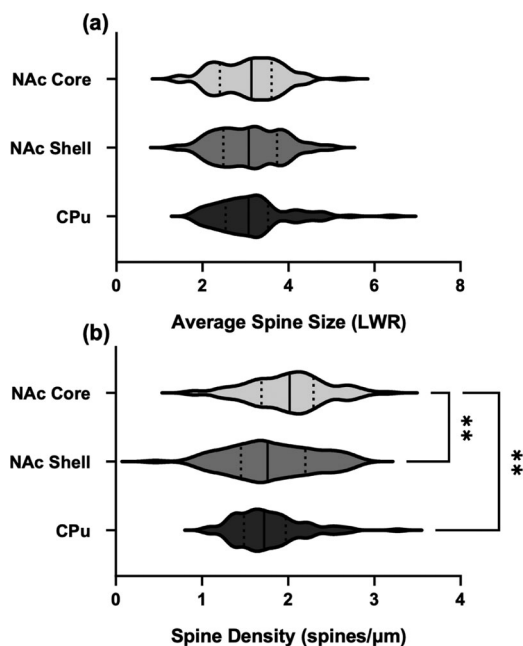


FIGURE 4 Dendritic spine density differed by striatal region independent of sex or estrous cycle phase. (a) Average spine size did not differ by striatal region. (b) Dendritic spine density is elevated in NAc core compared to NAc shell and CPu. LWR, length:width ratio; ***p* < .01.

3.3 | Overall spine size differed across estrous cycle phases in female NAc core and NAc shell, and spine length differed in NAc shell and CPu

Female rats exhibit an estrous cycle. Thus, we tested the hypothesis that spine attributes differed by estrous cycle phase within each striatal region. In the NAc core, overall spine size was decreased in proestrus PM compared to proestrus AM (Figure 6a) ($F(3,69) = 3.318$, $p = .0248$; diestrus: 3.083 ± 0.1478 , $n = 24$; proestrus AM: 3.391 ± 0.1843 , $n = 15$; proestrus PM: 2.687 ± 0.1571 , $n = 23$; estrus: 3.208 ± 0.1768 , $n = 11$). Within NAc shell, overall spine size for both proestrus PM and diestrus was decreased when compared to estrus (Figure 6b) ($F(3,69) = 2.927$, $p = .0398$; diestrus: 2.926 ± 0.1486 , $n = 24$; proestrus AM: 3.075 ± 0.2506 , $n = 13$; proestrus PM: 2.758 ± 0.1558 , $n = 19$; estrus: 3.472 ± 0.1832 ,

$n = 17$). There were no differences in overall spine size between estrous cycle phases within the CPu (Figure 6c) ($F(3,61) = 1.850$, $p = .1476$; diestrus: 2.976 ± 0.1451 , $n = 20$; proestrus AM: 3.315 ± 0.2595 , $n = 11$; proestrus PM: 2.872 ± 0.1755 , $n = 19$; estrus: 3.349 ± 0.1398 , $n = 15$). No differences were detected across estrous cycle phases for spine density in the NAc core (Figure 6d), NAc shell (Figure 6e), and CPu (Figure 6f) (NAc core: $F(3,69) = 0.7434$, $p = .5298$; NAc shell: $F(3,69) = 0.2255$, $p = .8784$; CPu: $F(3,61) = 0.8993$, $p = .4469$), indicating that spine density is not sensitive to the estrous cycle within these striatal regions. These data show that overall spine size is sensitive to the estrous cycle in the NAc core and NAc shell.

Given that changes were detected in spine size but not spine density, we further disaggregated the spine size data set by length and width. Average spine length within the NAc core trended toward a decrease in proestrus PM when compared to proestrus AM and estrus phases (Figure 7a) ($F(3,69) = 2.240$, $p = .0913$; diestrus: 1.300 ± 0.04776 , $n = 24$; proestrus AM: 1.424 ± 0.08085 , $n = 15$; proestrus PM: 1.221 ± 0.06692 , $n = 23$; estrus: 1.447 ± 0.09606 , $n = 11$). Within the NAc shell, average spine length was elevated in estrus compared to all other phases (Figure 7b) ($F(3,69) = 4.099$, $p = .0098$; diestrus: 1.220 ± 0.05634 , $n = 24$; proestrus AM: 1.254 ± 0.08016 , $n = 13$; proestrus PM: 1.154 ± 0.06211 , $n = 19$; estrus: 1.470 ± 0.07551 , $n = 17$). Within the CPu, both proestrus PM and diestrus average spine length was decreased compared to estrus (Figure 7c) ($F(3,61) = 3.138$, $p = .0317$; diestrus: 1.222 ± 0.05051 , $n = 20$; proestrus AM: 1.376 ± 0.1061 , $n = 11$; proestrus PM: 1.246 ± 0.05632 , $n = 19$; estrus: 1.460 ± 0.05864 , $n = 15$). Interestingly, no differences in average spine width across estrous cycle phases were found within the NAc core (Figure 7d), NAc shell (Figure 7e), or CPu (Figure 7f) (NAc core: $F(3,69) = 0.9723$, $p = .4109$; NAc shell: $F(3,69) = 0.1628$, $p = .9210$; CPu: $F(3,61) = 0.2449$, $p = .8647$). Spine length, not width, is sensitive to the estrous cycle within the NAc and CPu.

3.4 | Dendritic spine types varied for males and females in each estrous cycle phase for NAc core, NAc shell, and CPu

The detected differences in spine size, especially length, indicated that spine type may also differ within a region within each phase. We categorized spines into the following types: filopodia, long thin, thin, stubby,

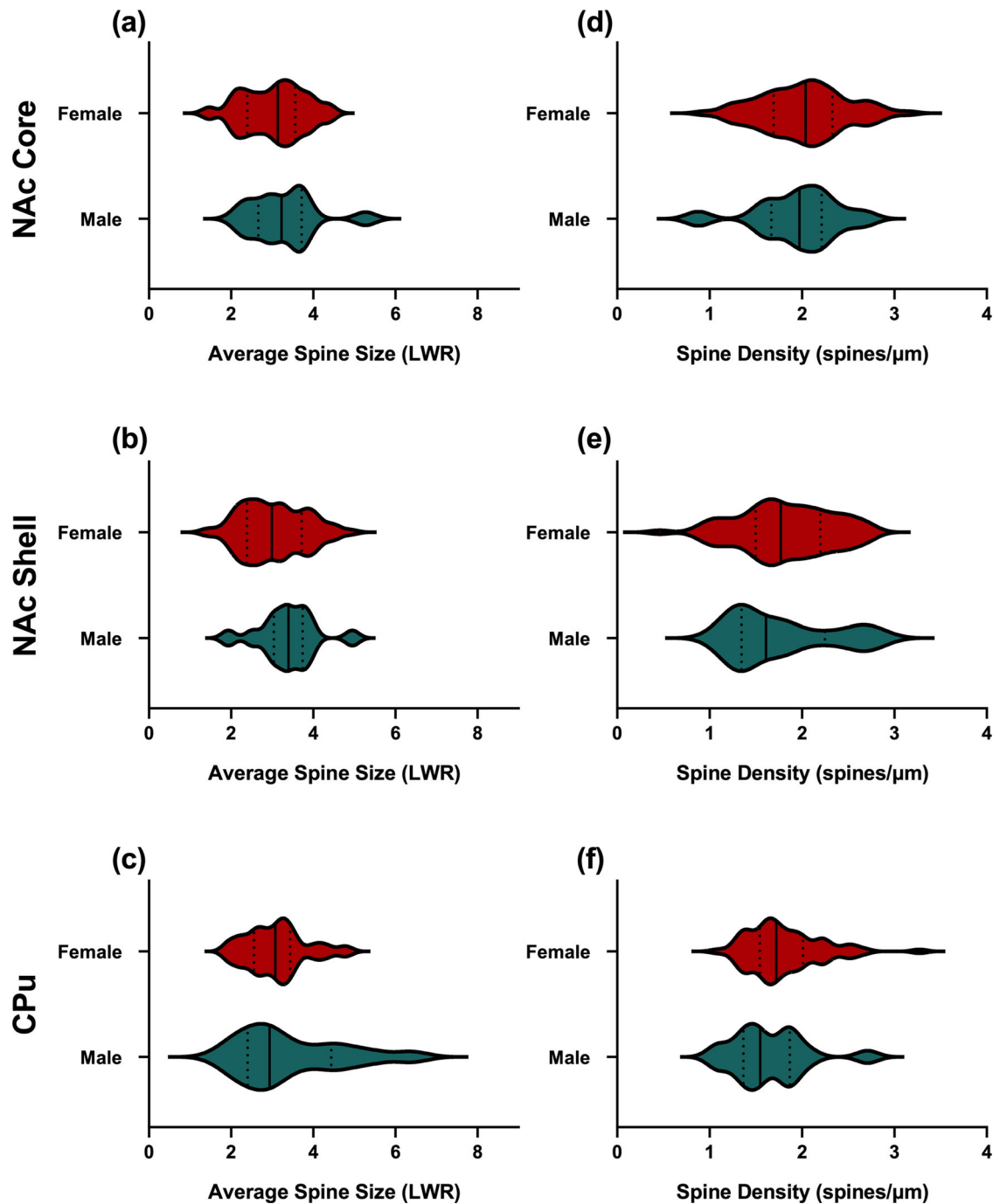


FIGURE 5 No differences in spine size or spine density by sex independent of estrous cycle phase. (a) NAc core spine size. (b) NAc shell spine size. (c) CPu spine size. (d) NAc core spine density. (e) NAc shell spine density. (f) CPu spine density. LWR, length:width ratio.

mushroom, and branched (Risher et al., 2014). Filopodia and long thin spine types represent the longest length spines of the six classifications. Stubby and thin spine types represent the shortest length spines of the six classifications. Mushroom spine types represent the widest spine type. We assessed the distribution of these spine types within a region for males and females in each estrous cycle phase. As expected, dendritic spine-type distribution differed within each group in the NAc core (Table 1), NAc shell (Table 2), and CPu (Table 3). Complete analysis is included in the respective tables. Here, we highlight relevant

comparisons as indicated from the results of the global spine size assessments presented above.

In the NAc core, global spine size assessment detected that overall spine size was smaller in proestrus PM compared to proestrus AM (Figure 6a). In proestrus PM, the percentage of spines classified as filopodia differed from long thin, thin, and branched (Table 1). The percentage of spines characterized as stubby differed from long thin and thin. In contrast, in proestrus AM, the percentage of spines classified as filopodia differed from long thin and stubby, while the percentage of

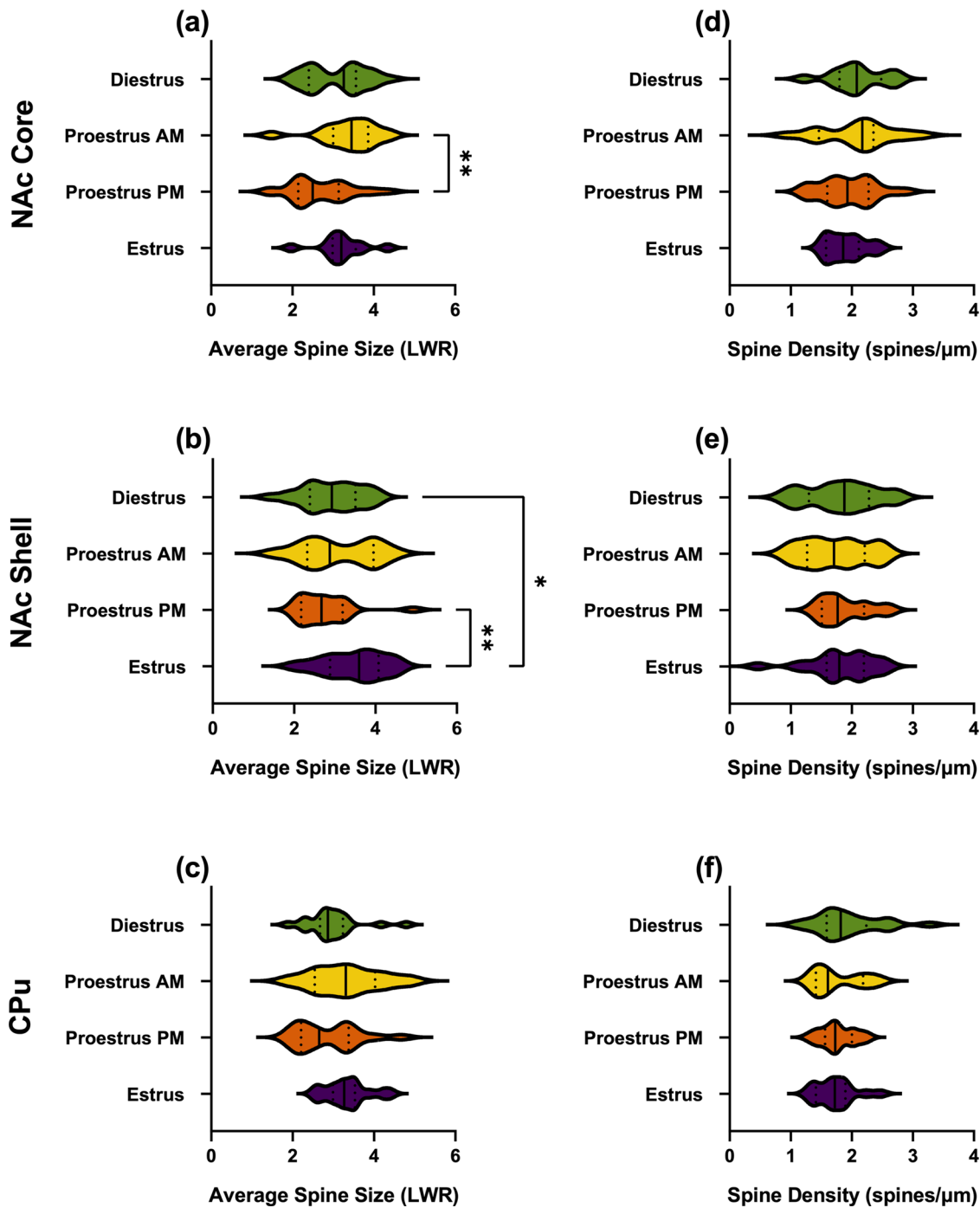


FIGURE 6 Overall dendritic spine size differed by estrous cycle phase in the NAc core and NAc shell, but not CPU. (a) In NAc core, average spine size was decreased in proestrus PM compared to proestrus AM. (b) In NAc shell, average spine size was increased in estrus compared to proestrus PM and diestrus. (c) CPU spine size. (d) NAc core spine density. (e) NAc shell spine density. (f) CPU spine density. LWR, length:width ratio; * $p < .05$; ** $p < .01$.

spines classified as stubby differed from filopodia, long thin, thin, and mushroom. These changing spine distributions are consistent with a shift toward shorter spine types in proestrus PM compared to AM.

In the NAc shell, overall spine length was greater in estrus compared to proestrus PM, proestrus AM, and diestrus (Figure 7b). In estrus, the percentage of spines classified as filopodia differed from long thin, stubby, and branched (Table 2). The percentage of spines classified

as stubby differed from filopodia, long thin, thin, and mushroom. In proestrus PM, the percentage of spines classified as filopodia differed from long thin and thin. The percentage of spines classified as stubby differed from long thin and thin. The percentage of spines classified as filopodia differed from long thin and thin. The percentage of spines classified as stubby differed from long thin and thin. In diestrus, the percentage of spines classified as

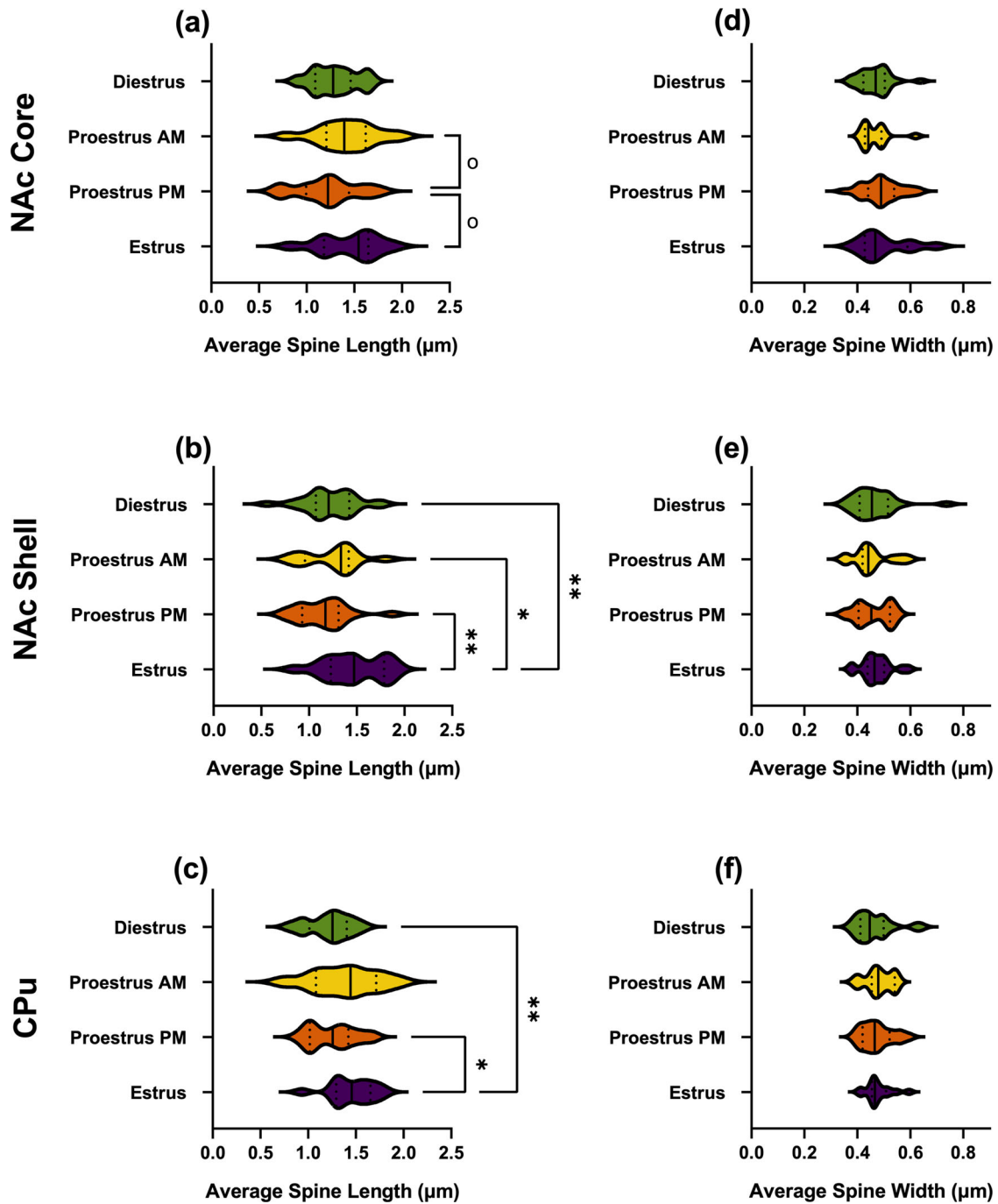


FIGURE 7 Average spine length differs by estrous cycle phase in the NAC shell and CPU, but not NAC core. (a) In NAC core, spine length trends lower in proestrus PM compared to both proestrus AM and estrus. (b) In NAC shell, spine length is elevated in estrus compared to all other phases. (c) In CPU, spine length is elevated in estrus compared to diestrus and proestrus PM. (d) NAC core spine width. (e) NAC shell spine width. (f) CPU spine width. $^{\circ}0.05 < p < .1$; $*p < .05$; $**p < .01$.

filopodia differed from long thin and thin. The percentage of spines classified as stubby differed from long thin, thin, and mushroom. The distribution of spine types in estrus is consistent with a greater spine length compared to the distributions in proestrus PM and diestrus.

In CPU, overall spine length was greater in estrus compared to proestrus PM, and diestrus (Figure 7c). In estrus, the percentage of spines classified as filopodia differed from long thin, stubby, and mush-

room (Table 3). The percentage of spines classified as stubby differed from filopodia, long thin, thin, mushroom, and branched. In proestrus PM, the percentage of spines classified as filopodia differed from long thin and thin. The percentage of spines classified as stubby differed from long thin, thin, and mushroom. In diestrus, the percentage of spines classified as filopodia differed from long thin, thin, and mushroom. The percentage of spines classified as stubby differed from long

TABLE 2 NAc shell dendritic spine types for males and females across estrous cycle phases.

	Filopodia	Long Thin	Thin	Stubby	Mushroom	Branched	Statistics (F, P)
Diestrus	9.9 ± 1.5 (24) ^{ab}	27.7 ± 3.4 (24) ^c	34.4 ± 3.0 (24) ^c	5.4 ± 1.4 (24) ^a	14.2 ± 2.2 (24) ^b	8.3 ± 2.1 (24) ^{ab}	3.290 × 10 ⁻¹² , <.0001
Proestrus AM	13.8 ± 2.4 (13) ^a	23.8 ± 3.3 (13) ^b	29.7 ± 3.2 (13) ^b	10.6 ± 2.4 (13) ^a	11.9 ± 3.1 (13) ^a	10.2 ± 2.2 (13) ^a	7.819 × 10 ⁻¹² , .0002
Proestrus PM	9.1 ± 2.0 (19) ^{ab}	30.4 ± 2.8 (19) ^c	33.5 ± 2.6 (19) ^c	7.4 ± 2.0 (19) ^a	14.3 ± 2.1 (19) ^b	5.3 ± 1.8 (19) ^a	5.539 × 10 ⁻¹² , <.0001
Estrus	19.3 ± 2.9 (17) ^{ab}	28.2 ± 2.6 (17) ^c	26.1 ± 3.6 (17) ^{ac}	4.7 ± 1.1 (17) ^d	13.5 ± 2.4 (17) ^{be}	8.1 ± 2.0 (17) ^{de}	3.167 × 10 ⁻¹² , <.0001
Males	16.4 ± 2.9 (15) ^{ab}	28.5 ± 2.7 (15) ^c	27.8 ± 4.6 (15) ^{bc}	4.6 ± 1.5 (15) ^d	9.5 ± 2.3 (15) ^{ad}	13.2 ± 1.9 (15) ^a	4.734 × 10 ⁻¹² , .0002

Note: Values are spine type percent of total, mean ± SEM. Numbers in parentheses indicate number of dendritic segments analyzed. Different superscript letters indicate statistically significant differences between dendritic spine types. Spine types with the same superscript letter do not significantly differ.

TABLE 3 CPu dendritic spine types for males and females across estrous cycle phases.

	Filopodia	Long Thin	Thin	Stubby	Mushroom	Branched	Statistics (F, P)
Diestrus	7.3 ± 1.7 (20) ^a	33.7 ± 2.7 (20) ^b	26.6 ± 2.3 (20) ^b	7.5 ± 2.0 (20) ^a	14.6 ± 1.4 (20) ^c	10.4 ± 1.9 (20) ^{ac}	6.93 × 10 ⁻¹² , <.0001
Proestrus AM	14.7 ± 3.6 (11) ^{ab,c}	29.4 ± 3.2 (11) ^d	29.0 ± 4.6 (11) ^{bd}	5.0 ± 2.5 (11) ^a	14.9 ± 1.9 (11) ^c	7.0 ± 3.0 (11) ^a	1.970 × 10 ⁻¹² , .0003
Proestrus PM	10.2 ± 2.2 (19) ^{ab}	34.6 ± 3.3 (19) ^c	26.3 ± 2.8 (19) ^c	8.7 ± 1.9 (19) ^a	14.9 ± 2.3 (19) ^b	5.3 ± 1.9 (19) ^a	6.287 × 10 ⁻¹² , <.0001
Estrus	20.2 ± 2.9 (15) ^{ab}	31.1 ± 2.5 (15) ^c	24.0 ± 2.5 (15) ^{ac}	3.7 ± 1.0 (15) ^e	10.2 ± 2.1 (15) ^d	10.8 ± 2.8 (15) ^{bd}	8.939 × 10 ⁻¹² , <.0001
Males	17.5 ± 4.3 (16) ^{ab}	32.5 ± 3.9 (16) ^c	26.9 ± 3.6 (16) ^{bc}	7.2 ± 1.5 (16) ^a	10.3 ± 3.2 (16) ^a	5.5 ± 2.3 (16) ^a	4.225 × 10 ⁻¹² , <.0001

Note: Values are spine type percent of total, mean ± SEM. Numbers in parentheses indicate number of dendritic segments analyzed. Different superscript letters indicate statistically significant differences between dendritic spine types. Spine types with the same superscript letter do not significantly differ.

thin, thin, and mushroom. Similar to the NAc shell, in the CPu the distribution of spine types in estrus is consistent with increased spine length compared to the distributions in proestrus PM and diestrus.

4 | DISCUSSION

These findings are the first to demonstrate MSN dendritic spine plasticity in response to the estrous cycle. Interestingly, the sensitivity of MSN dendritic spines to estrous cycle phase notably differs across striatal regions and in specific dendritic spine size attributes. In the NAc core, overall spine size was decreased in proestrus PM compared to proestrus AM. In the NAc shell, overall spine size was elevated in estrus compared to proestrus PM and diestrus. Spine length differed across estrous cycle phases in female NAc shell and CPu. In the NAc shell, spine length was elevated in estrus compared to diestrus, proestrus AM, and proestrus PM. In the CPu, spine length was elevated in estrus compared to diestrus and proestrus PM. These findings indicate that rapid changes in spine attributes can occur within hours between proestrus AM and PM in specific regions of the adult rat striatum. Independent of sex or estrous cycle phase, dendritic spine density was greater in the NAc core compared to both the NAc shell and CPu, recapitulating previous findings and validating our approach (Bello-Medina et al., 2016; Forlano & Woolley, 2010; Meredith et al., 1992; Staffend et al., 2011; Wissman et al., 2011).

Our work directly extends previous findings regarding the intersection of spine attributes with natural variables such as sex, estrous cycle phases, and estradiol in the striatal regions (Almey et al., 2012,

2015, 2022; Forlano & Woolley, 2010; Gross et al., 2016; Peterson et al., 2015a, 2016; Staffend et al., 2011; Wissman et al., 2011, 2012). While no study before this one has directly tested the hypothesis that MSN dendritic spine attributes are sensitive to the estrous cycle, previous experiments from other laboratories have demonstrated that MSN spines are sensitive to estradiol. Treatment of ovariectomized female hamsters and rats with estradiol resulted in decreased spine density in the NAc core (Peterson et al., 2015a; Staffend et al., 2011), concomitant with a shift from more mature to less mature spine types (Staffend et al., 2011), similar to what was later reported in the perirhinal cortex (Gervais et al., 2015). Spine size was not assessed in these studies. With MSN dendritic spine plasticity previously linked to estradiol exposure, we hypothesized that spine attributes would differ across the estrous cycle. This initial hypothesis was informed by previous experiments from Woolley and colleagues that detected sex differences in specific spine attributes and glutamatergic synapse markers between male and female rats from the proestrus phase (other phases were not examined) (Forlano & Woolley, 2010; Wissman et al., 2011, 2012).

Surprisingly, we found that spine size rather than spine density differed across estrous cycle phases. Our use of the Golgi process may have detected smaller spine sizes that might have not been apparent with a different technique such as the DiOlistic labeling employed in earlier studies (Forlano & Woolley, 2010; Peterson et al., 2015a, 2016; Staffend et al., 2011, 2014). The current study also by necessity employed a different mounting media than earlier studies where DiOlistic labeling was used. Mounting media has been shown to influence dendritic spine density measurements (Peterson et al., 2015b). These differences in technique may have resulted in a detected shift

in spine size rather than density in our data. We favor this possibility as the most likely explanation as to why the current study detected a decrease in spine size rather than spine density. Other alternative explanations exist. One is spine distance relative to the soma. Though the range of distance to soma overlaps that of earlier studies of estradiol impacts on NAc MSN spine plasticity (Peterson et al., 2016; Staffend et al., 2011), it is possible that our studies differentially sampled distance to soma and/or primary and secondary dendrites. Spines could potentially exhibit greater dynamics along the proximal to distal plane or in secondary compared to primary dendrites. These facets were not recorded as an experimental variable in these studies. Another potential explanation is that progesterone or some other relevant hormone also regulates spine attributes, resulting in differential results in dendritic spine properties than when estradiol is considered alone. Alternatively, Woolley and colleagues previously reported that rostrocaudal location within the NAc core played a role in detection of sex differences with differences in spine density between males and females in proestrus only evident in the caudal NAc core (Bregma 1.44–1.0), and spine head width, a measure of spine size, only differing in the rostral NAc core (Bregma 2.0–1.56) (Wissman et al., 2012). Since we sampled MSNs mostly from Bregma 1.92 to 1.44, it is possible that spine size varies only within these rostral portions of the NAc core, NAc shell, and CPU. Further experiments utilizing additional samples from the caudal portions of the NAc core, as well as the NAc shell and CPU, should be performed to gain a more comprehensive view of spine plasticity by estrous cycle phase. Future CPU studies could also disaggregate by subregion, which was not performed in the current study and this heterogeneity could potentially have obscured potential effects of sex hormones on dendritic spine. To gain maximum insight, we recommend that these future studies evaluate both spine density and global spine size, as well as specific spine size attributes, including both length and width.

One important conclusion from this study is that a rapid change in spine attributes occurs within hours between proestrus AM and PM in specific regions of the adult rat striatum, and then recovers by the next morning of estrus, a remarkable shift similar to previously detected changes across the estrous cycle in the hippocampus (Brandt et al., 2020; Woolley et al., 1990), but never before in a striatal region. This rapid change in spine size is further upheld by the shifts in spine types assessed within each phase of the estrous cycle for NAc core, NAc shell, and CPU. A qualitative analysis of the relationships between spine type proportions provides insight into these shifts between estrous cycle phases (Figure 8). This analysis was pursued within each region, including males and females in each estrous cycle phase. In the NAc core (Figure 8a), the relationship between spine type proportions changes from phase to phase. For example, proestrus AM features a relatively larger proportion of long spine types, such as filopodia and long thin. Proestrus PM features a relatively larger proportion of short spine types, such as thin and stubby. Another interesting pattern also emerges from this analysis of the NAc core: males and females in diestrus exhibit an identical pattern of relationships between spine-type proportions, as indicated by the same line array in Figure 8a. Consistent with this conclusion, males and females in

diestrus also share similar percentages of each spine type (Table 1). This observation corresponds to data indicating that the electrophysiological properties of NAc core MSNs from females in the diestrus phase are similar to males, unlike MSNs recorded during other estrous cycle phases (Proaño et al., 2018, 2020). Regarding the NAc shell, this analysis provides several relevant observations (Figure 8b). In the NAc shell, estrus features a relatively larger proportion of long spine types compared to short spine types, which is different from all other phases. For example, both diestrus and proestrus PM show a larger proportion of short spine types compared to long spine types. The relationships between spine type proportions within each of these phases closely resemble one another. Proestrus AM features a more equal distribution of spine type proportions than any other phase, as indicated by smaller weighted and/or missing relationship lines. These differences in spine type proportion relationships between proestrus AM and other phases could explain why no global spine size differences were detected (Figure 7b). In the CPU (Figure 8c), estrus features a relatively larger proportion of long spine types compared to short spine types. In contrast, diestrus and proestrus PM both feature a relatively larger proportion of short spine types, namely stubby, compared to long spine types, namely filopodia. Similar to the NAc shell, proestrus AM in the CPU features few significant differences between spine-type proportions. Overall, this analysis of spine-type distribution is consistent with findings that global spine size and length are sensitive to estrous cycle phase in select striatal regions.

Differences in spine size across the estrous cycle are also significant in that they align with previous electrophysiological experiments, especially in the NAc core. Whole-cell patch clamp recordings of NAc core MSNs discovered that the frequency and amplitude of mEPSCs change across the estrous cycle. mEPSCs in recording configuration employed by these experiments are a direct functional assessment of AMPA receptor-mediated synapses and can correlate with dendritic spine attributes. Specifically, mEPSC frequency is intermediate during diestrus, increases during proestrus AM, plummets during proestrus PM, and increases again during estrus (Proaño et al., 2018, 2020). This decrease in mEPSC frequency during proestrus PM directly aligns with the detected decrease in spine size in proestrus PM, suggesting a neuroanatomical mechanism. Importantly, mEPSC frequency is typically interpreted as an indicator of the number of available active glutamatergic synapse. It is a logical model that as dendritic spine size decreases, the number of active glutamatergic synapses will likewise decrease, resulting in a lower mEPSC frequency. Consistent with this model, mEPSC frequency inversely correlates with circulating concentrations of estradiol and progesterone, both of which would be higher during the proestrus PM phase compared to most other phases. This correlation has been tested causally by the application of estradiol directly onto MSN neurons while recording mEPSCs. Female but not male MSNs lower mEPSC frequency in response to estradiol exposure (Proaño et al., 2018). Interestingly, mEPSC amplitude in NAc core MSNs also changes across the estrous cycle. mEPSC amplitude is typically indicative of changes at the postsynaptic side of the synapse, for instance, in the number of AMPA receptors per synapse. mEPSC amplitude is intermediate during the diestrus and proestrus AM phases,

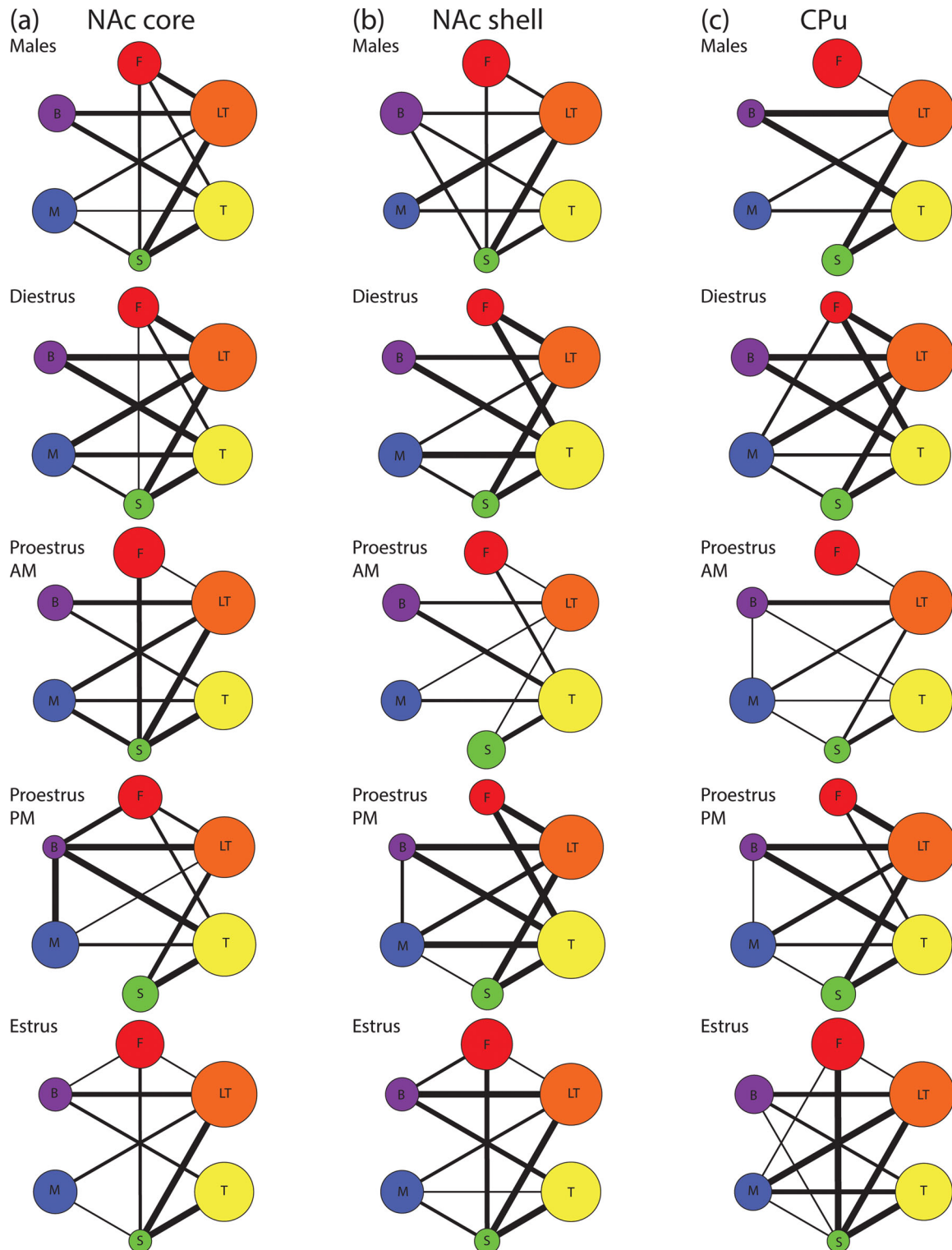


FIGURE 8 Visual representation of spine type distributions for males and females of each estrous cycle phase. (a) NAc core. (b) NAc shell. (c) CPu. This representation demonstrates region-specific differences in the impact of the estrous cycle upon dendritic spine type. For example, in the NAc core, proestrus AM features a relatively larger proportion of long spine types, such as filopodia and long thin, while proestrus PM features a relatively larger proportion of short spine types, such as thin and stubby. Circle diameter indicates spine type proportion, with larger diameters indicating increased proportion. Circle color corresponds with spine type. Connecting lines between spine type circles indicate the presence of a statistically significant difference between proportions. Lack of a line indicates no significant difference exists in proportion between the respective spine types. Line weight represents p value, with increasing weight indicating decreasing p value. Quantitative metrics are provided in Tables 2–3. F, filopodia; LT, long thin; T, thin; S, stubby; M, mushroom; B, branched.

increases during proestrus PM, and returns to intermediate levels during estrus (Proaño et al., 2018, 2020). NAc core MSN mEPSC amplitude correlates with circulating concentrations of estradiol and progesterone, and in both females and males is weakly sensitive to acute exogenous estradiol exposure. Thus, it is possible that the changes in dendritic spine size observed in NAc core proestrus PM in the present study reduce the number of available synapses, leading to a decrease in mEPSC frequency, and either potentiate the remaining synapse or simply eliminate weaker synapse, leading to the increase in mEPSC amplitude. The current study also detects differences in spine length across the estrous cycle in CPu. Longer spines were measured in estrus compared to diestrus and proestrus PM. Unlike the NAc core, the functional relevance of the changes in CPu spine length are not as clear. One previous study assessed mEPSC properties across the estrous cycle in CPu MSN; however, no changes in mEPSC properties were detected (Willett et al., 2020). Concerning the NAc shell, to our knowledge there have been no studies of synaptic physiology across the estrous cycle, or comparing by sex in adult animals to complement a previous study of prepubertal animals (Willett et al., 2016). We recommend that studies of synaptic physiology in the NAc shell across estrous cycle phases should be performed given that differences in spine size were detected in this brain region.

At this point, the mechanism driving rapid changes in spine size remains unknown. Several pertinent possibilities exist. One possibility derives from a model first articulated by Mermelstein, Meisel, and colleagues. In their experiments, changes in spine attributes in gonadectomized female rat NAc core induced by exogenous estradiol administration were mediated via an estrogen receptor (ER)-associated mGluR5/endocannabinoid pathway that initiates on the postsynaptic side of the synapse on the medium spiny neuron (Gross et al., 2016; Peterson et al., 2015a, 2016; Staffend et al., 2011). The natural changes in spine attributes across the estrous cycle may also be mediated via this same pathway. Membrane-associated ERs are anatomically situated on medium spiny neurons, dopaminergic terminals (depending striatal region), GABAergic terminals, and potentially glutamatergic terminals, although glutamatergic terminals have not yet been confirmed (Krentzel et al., 2019) (Almey et al., 2012, 2016, 2022); localizations are consistent with this model. To help drive future experiments, we have developed an additional speculative model for how estrous cycle-associated dendritic spine plasticity may be derived. We hypothesize that the estradiol peak in proestrus AM creates a delayed effect on dendritic spines that is measurable in the proestrus PM hours. This is seen in the data as a rapid reduction in spine size, particularly length, between proestrus AM and proestrus PM. This estradiol influence on dendritic spine size may be mediated through membrane-associated ERs on the presynaptic side of the synapse, as ERs are more abundant on the presynaptic side of NAc core and shell synapses (Almey et al., 2022), perhaps inducing a delayed effect on spine size through altering neurotransmitter release (Micevych & Christensen, 2012). There may also be actions via ER activation on the postsynaptic side of the synapse, as MSNs express ERs in that location and in the soma (Almey et al., 2012, 2016, 2022; Krentzel et al., 2019). We note that these two models are not mutually exclu-

sive, and that estradiol might initiate modulation on both the presynaptic and postsynaptic sides of the synapse.

Importantly, the ER/mGluR5/endocannabinoid model articulated in previous publications focuses on estradiol action and does not include other key hormones such as progesterone. Changes in mEPSC properties are correlated with circulating plasma progesterone concentrations, and the estrous cycle phase with some of the greatest changes in spine attributes is proestrus PM, when progesterone concentrations are high (Proaño et al., 2020; Woolley & McEwen, 1993). Woolley and McEwen (1993) and Murphy and Segal (2000) observed that progesterone rapidly attenuated estradiol effects on dendritic spine density *in vivo* in ovariectomized rat CA1 hippocampus and in cultured hippocampal neurons, respectively. To our knowledge, progesterone's effects on spine attributes have not been investigated in the striatum. With this in mind, our speculative model hypothesizes that the peak in progesterone occurring in proestrus PM rapidly attenuates estradiol's delayed effects on spine properties, seen in the data as an increase in spine size in estrus compared to proestrus PM. To test the hypotheses that progesterone rapidly attenuates estradiol's delayed effects on MSN dendritic spine attributes, it would be beneficial to conduct an experiment much like Woolley and McEwen's by introducing estradiol and/or progesterone to gonadectomized male and female rats to determine the timed effects on MSN dendritic spines. A future study could also examine the naturally cycling animal's temporal cytoskeletal markers from striatal tissue at various stages of the estrous cycle, particularly before, during, and after estradiol and progesterone surges occurring in proestrus AM and PM and continuing effects in estrus.

Changes in MSN dendritic spine dynamics could also interact with dopaminergic action. We found that spine length rather than spine head width drove differences across the estrous cycle. Dendritic spine necks are often sites for dopaminergic input onto MSNs and dopamine levels are implicated in regulating spine attributes, at least in the CPu (Alberquilla et al., 2020; Arbuthnott et al., 2000). Decades of literature implicate estradiol in altering dopamine signaling dynamics in the striatum (Yoest et al., 2018). While there are data regarding changing dopamine levels and the estrous cycle (Dluzen & Ramirez, 1985; Xiao & Becker, 1994), to our knowledge it is unknown how dopamine levels change between proestrus AM and proestrus PM in any striatal region. We also note that MSNs differentially express dopamine receptors, creating MSN subtypes that could exhibit differential responsiveness to estrous cycle phase (Calipari et al., 2016; Staffend et al., 2014). We recommend that this be addressed, since it holds ramifications for both natural processes and relevant disorders. Thus, another line of future investigation could be centered around dopamine's involvement in estrous cycle-associated spine dynamics, and how dopamine and glutamate interact to produce spine changes.

In conclusion, these data generate the following conclusions that revise our understanding of the dynamics of dendritic spines in the striatal regions. 1. MSN dendritic spine size is sensitive to estrous cycle phase. 2. When estrous cycle was not taken into account as a biological variable, there were no detected sex differences in spine attributes. 3. Spine size attributes rapidly shift between cycle phases in a matter of hours, mirroring equally rapid shifts in electrophysiology as well

as relevant behaviors. It has long been documented that behaviors modulated by the striatal regions, especially motivated locomotor and reproductive-related behaviors influenced by NAc, can rapidly change between estrous cycle phases or exposure to estradiol (Krentzel et al., 2020; Meitzen et al., 2018; Yoest et al., 2018). Thus, it is tempting to speculate that the structural dynamics observed here hold strong implications for function and behavioral output, although the ultimate function is not yet known. Nevertheless, the findings presented here provide important information, linking previous work establishing the sexually differentiated nature of MSN dendritic spines and glutamatergic input, studies that employed gonadectomized animals and exogenous estradiol replacement paradigms to assess MSN dendritic spine attributes and elucidate underlying molecular mechanisms, and electrophysiological studies upon MSNs in naturally cycling females across estrous cycle phases.

AUTHOR CONTRIBUTIONS

Anna L. S. Beeson designed the experiments, collected data, analyzed data, and contributed to drafts of the manuscript. John Meitzen designed the experiments, analyzed data, and contributed to drafts of the manuscript. Both authors read and approved the final draft of the manuscript.

ACKNOWLEDGMENTS

We thank Opal Patel, Natalie Truby, and Laura Ginnari for help with protocol development and pilot experiments; David Dorris for microscopy and technical support; Dr. Christiana Miller and Dr. Stephanie Proaño for estrous cycle training; Dr. Amanda Krentzel for statistical consultation; Dr. Jinyan Cao for neuroanatomy training; and Dr. Scott Belcher for the use of his laboratory's microscope and advice concerning objectives.

CONFLICT OF INTEREST STATEMENT

The authors declare no conflicts of interest.

DATA AVAILABILITY STATEMENT

The data that support the findings of this study are available from the corresponding author upon reasonable request.

ORCID

Anna L. S. Beeson  <https://orcid.org/0000-0002-9839-0726>

John Meitzen  <https://orcid.org/0000-0002-8860-4110>

PEER REVIEW

The peer review history for this article is available at <https://publons.com/publon/10.1002/cne.25460>.

REFERENCES

- Adams, C., Chen, X., & Moenter, S. M. (2018). Changes in GABAergic transmission to and intrinsic excitability of gonadotropin-releasing hormone (GnRH) neurons during the estrous cycle in mice. *eNeuro*, 5, ENEURO.0171-18.2018.
- Ajayi, A. F., & Akhigbe, R. E. (2020). Staging of the estrous cycle and induction of estrus in experimental rodents: An update. *Fertility Research and Practice*, 6, 5.
- Alberquilla, S., Gonzalez-Granillo, A., Martín, E. D., & Moratalla, R. (2020). Dopamine regulates spine density in striatal projection neurons in a concentration-dependent manner. *Neurobiology of Disease*, 134, 104666.
- Almei, A., Filardo, E. J., Milner, T. A., & Brake, W. G. (2012). Estrogen receptors are found in glia and at extranuclear neuronal sites in the dorsal striatum of female rats: Evidence for cholinergic but not dopaminergic colocalization. *Endocrinology*, 153, 5373–5383.
- Almei, A., Milner, T. A., & Brake, W. G. (2015). Estrogen receptors in the central nervous system and their implication for dopamine-dependent cognition in females. *Hormones and Behavior*, 74, 125–138.
- Almei, A., Milner, T. A., & Brake, W. G. (2016). Estrogen receptor α and G-protein coupled estrogen receptor 1 are localized to GABAergic neurons in the dorsal striatum. *Neuroscience Letters*, 622, 118–123.
- Almei, A., Milner, T. A., & Brake, W. G. (2022). Estrogen receptors observed at extranuclear neuronal sites and in glia in the nucleus accumbens core and shell of the female rat: Evidence for localization to catecholaminergic and GABAergic neurons. *Journal of Comparative Neurology*, 530(11), 2056–2072.
- Arbuthnott, G. W., Ingham, C. A., & Wickens, J. R. (2000). Dopamine and synaptic plasticity in the neostriatum. *Journal of Anatomy*, 196, 587–596.
- Bello-Medina, P. C., Flores, G., Quirarte, G. L., McGaugh, J. L., & Prado Alcalá, R. A. (2016). Mushroom spine dynamics in medium spiny neurons of dorsal striatum associated with memory of moderate and intense training. *Proceedings National Academy of Science of the United States of America*, 113(42), E6516–E6525.
- Brandt, N., Löffler, T., Fester, L., & Rune, G. M. (2020). Sex-specific features of spine densities in the hippocampus. *Scientific Reports*, 10, 11405.
- Calipari, E. S., Bagot, R. C., Purushothaman, I., Davidson, T. J., Yorgason, J. T., Peña, C. J., Walker, D. M., Pirpinias, S. T., Guise, K. G., Ramakrishnan, C., Deisseroth, K., & Nestler, E. J. (2016). In vivo imaging identifies temporal signature of D1 and D2 medium spiny neurons in cocaine reward. *Proceedings National Academy of Science of the United States of America*, 113, 2726–2731.
- Chen, J.-R., Yan, Y.-T., Wang, T.-J., Chen, L.-J., Wang, Y.-J., & Tseng, G.-F. (2009). Gonadal hormones modulate the dendritic spine densities of primary cortical pyramidal neurons in adult female rat. *Cerebral Cortex*, 19, 2719–2727.
- Dluzen, D., & Ramirez, V. D. (1985). In vitro dopamine release from the rat striatum: Diurnal rhythm and its modification by the estrous cycle. *Neuroendocrinology*, 41, 97–100.
- Fiala, J. C. (2005). Reconstruct: A free editor for serial section microscopy. *Journal of Microscopy*, 218, 52–61.
- Floresco, S. B. (2015). The nucleus accumbens: An interface between cognition, emotion, and action. *Annual Review of Psychology*, 66, 25–52.
- Forlano, P. M., & Woolley, C. S. (2010). Quantitative analysis of pre- and postsynaptic sex differences in the nucleus accumbens. *Journal of Comparative Neurology*, 518(8), 1330–1348.
- Freeman, M. E. (1994). The neuroendocrine control of the ovarian cycle of the rat. *The Physiology of Reproduction*, 2, 613–658.
- Gervais, N. J., Mumby, D. G., & Brake, W. G. (2015). Attenuation of dendritic spine density in the perirhinal cortex following 17 β -Estradiol replacement in the rat: E2 and dendritic spines in the PRH of female rats. *Hippocampus*, 25, 1212–1216.
- González-Burgos, I., Velázquez-Zamora, D. A., González-Tapia, D., & Cervantes, M. (2015). A Golgi study of the plasticity of dendritic spines in the hypothalamic ventromedial nucleus during the estrous cycle of female rats. *Neuroscience*, 298, 74–80.
- Graybiel, A. M., & Grafton, S. T. (2015). The striatum: Where skills and habits meet. *Cold Spring Harbor Perspectives in Biology*, 7, a021691.

- Gross, K. S., Brandner, D. D., Martinez, L. A., Olive, M. F., Meisel, R. L., & Mermelstein, P. G. (2016). Opposite effects of mGluR1a and mGluR5 activation on nucleus accumbens medium spiny neuron dendritic spine density. *PLoS ONE*, *11*, e0162755.
- Harte-Hargrove, L. C., Varga-Wesson, A., Duffy, A. M., Milner, T. A., & Scharfman, H. E. (2015). Opioid receptor-dependent sex differences in synaptic plasticity in the hippocampal mossy fiber pathway of the adult rat. *Journal of Neuroscience*, *35*, 1723–1738.
- Hashimoto, I., Isomoto, N., Eto, M., Kawaminami, M., Sunazuka, C., & Ueki, N. (1987). Preovulatory secretion of progesterone, luteinizing hormone, and prolactin in 4-day and 5-day cycling rats. *Biology of Reproduction*, *36*, 599–605.
- Hubscher, C., Brooks, D., & Johnson, J. (2005). A quantitative method for assessing stages of the rat estrous cycle. *Biotechnic & Histochemistry*, *80*, 79–87.
- Jackson, T. W., Ryherd, G. L., Scheibly, C. M., Sasser, A. L., Guillette, T. C., & Belcher, S. M. (2020). Gestational CD exposure in the CD-1 mouse induces sex-specific hepatic insulin insensitivity, obesity, and metabolic syndrome in adult female offspring. *Toxicological Sciences*, *178*, 264–280.
- Krentzel, A. A., Barrett, L. R., & Meitzen, J. (2019). Estradiol rapidly modulates excitatory synapse properties in a sex- and region-specific manner in rat nucleus accumbens core and caudate-putamen. *Journal of Neurophysiology*, *122*, 1213–1225.
- Krentzel, A. A., Proaño, S., Patisaul, H. B., & Meitzen, J. (2020). Temporal and bidirectional influences of estradiol on voluntary wheel running in adult female and male rats. *Hormones and Behavior*, *120*, 104694.
- Landeros, R. V., Morisseau, C., Yoo, H. J., Fu, S. H., Hammock, B. D., & Trainor, B. C. (2012). Corn cob bedding alters the effects of estrogens on aggressive behavior and reduces estrogen Receptor- α expression in the brain. *Endocrinology*, *153*, 949–953.
- Mani, S. K., Reyna, A. M., Alejandro, M. A., Crowley, J., & Markaverich, B. M. (2005). Disruption of male sexual behavior in rats by tetrahydrofurandiols (THF-diols). *Steroids*, *70*, 750–754.
- Meitzen, J., Meisel, R. L., & Mermelstein, P. G. (2018). Sex differences and the effects of estradiol on striatal function. *Current Opinion in Behavioral Sciences*, *23*, 42–48.
- Meredith, G. E., Agolia, R., Arts, M. P. M., Groenewegen, H. J., & Zahm, D. S. (1992). Morphological differences between projection neurons of the core and shell in the nucleus accumbens of the rat. *Neuroscience*, *50*, 149–162.
- Micevych, P., & Christensen, A. (2012). Membrane-initiated estradiol actions mediate structural plasticity and reproduction. *Frontiers in Neuroendocrinology*, *33*, 331–341.
- Micevych, P. E., & Meisel, R. L. (2017). Integrating neural circuits controlling female sexual behavior. *Frontiers in Systems Neuroscience*, *11*, 42.
- Micevych, P. E., Mermelstein, P. G., & Sinchak, K. (2017). Estradiol membrane-initiated signaling in the brain mediates reproduction. *Trends in Neurosciences*, *40*, 654–666.
- Murphy, D. D., & Segal, M. (2000). Progesterone prevents estradiol-induced dendritic spine formation in cultured hippocampal neurons. *Neuroendocrinology*, *72*, 133–143.
- Paxinos, G., & Watson, C. (2005). *The rat brain in stereotaxic coordinates* (5th ed.) Academic Press.
- Peterson, B. M., Martinez, L. A., Meisel, R. L., & Mermelstein, P. G. (2016). Estradiol impacts the endocannabinoid system in female rats to influence behavioral and structural responses to cocaine. *Neuropharmacology*, *110*, 118–124.
- Peterson, B. M., Mermelstein, P. G., & Meisel, R. L. (2015a). Estradiol mediates dendritic spine plasticity in the nucleus accumbens core through activation of mGluR5. *Brain Structure and Function*, *220*, 2415–2422.
- Peterson, B. M., Mermelstein, P. G., & Meisel, R. L. (2015b). Impact of immersion oils and mounting media on the confocal imaging of dendritic spines. *Journal of Neuroscience Methods*, *242*, 106–111.
- Proaño, S. B., Krentzel, A. A., & Meitzen, J. (2020). Differential and synergistic roles of 17 β -estradiol and progesterone in modulating adult female rat nucleus accumbens core medium spiny neuron electrophysiology. *Journal of Neurophysiology*, *123*, 2390–2405.
- Proaño, S. B., Morris, H. J., Kunz, L. M., Dorris, D. M., & Meitzen, J. (2018). Estrous cycle-induced sex differences in medium spiny neuron excitatory synaptic transmission and intrinsic excitability in adult rat nucleus accumbens core. *Journal of Neurophysiology*, *120*, 1356–1373.
- Rasia-Filho, A. A., Fabian, C., Rigoti, K. M., & Achaval, M. (2004). Influence of sex, estrous cycle and motherhood on dendritic spine density in the rat medial amygdala revealed by the Golgi method. *Neuroscience*, *126*, 839–847.
- Risher, W. C., Ustunkaya, T., Singh Alvarado, J., & Eroglu, C. (2014). Rapid Golgi analysis method for efficient and unbiased classification of dendritic spines. *PLoS ONE*, *9*, e107591.
- Rosoklija, G. B., Petrushevski, V. M., Stankov, A., Dika, A., Jakovski, Z., Pavlovski, G., Davcheva, N., Lipkin, R., Schnieder, T., Scobie, K., Duma, A., & Dwork, A. J. (2014). Reliable and durable Golgi staining of brain tissue from human autopsies and experimental animals. *Journal of Neuroscience Methods*, *230*, 20–29.
- Scharfman, H. E., Hintz, T. M., Gomez, J., Stormes, K. A., Barouk, S., Malthankar-Phatak, G. H., McCloskey, D. P., Luine, V. N., & MacLusky, N. J. (2007). Changes in hippocampal function of ovariectomized rats after sequential low doses of estradiol to simulate the preovulatory estrogen surge: Hippocampal effects of preovulatory estradiol levels. *European Journal of Neuroscience*, *26*, 2595–2612.
- Scharfman, H. E., & MacLusky, N. J. (2006). Estrogen and brain-derived neurotrophic factor (BDNF) in hippocampus: Complexity of steroid hormone-growth factor interactions in the adult CNS. *Frontiers in Neuroendocrinology*, *27*, 415–435.
- Scharfman, H. E., Mercurio, T. C., Goodman, J. H., Wilson, M. A., & MacLusky, N. J. (2003). Hippocampal excitability increases during the estrous cycle in the rat: A potential role for brain-derived neurotrophic factor. *Journal of Neuroscience*, *23*, 11641–11652.
- Schwarz, J. M., Liang, S.-L., Thompson, S. M., & McCarthy, M. M. (2008). Estradiol induces hypothalamic dendritic spines by enhancing glutamate release: A mechanism for organizational sex differences. *Neuron*, *58*, 584–598.
- Staffend, N. A., Hedges, V. L., Chemel, B. R., Watts, V. J., & Meisel, R. L. (2014). Cell-type specific increases in female hamster nucleus accumbens spine density following female sexual experience. *Brain Structure and Function*, *219*, 2071–2081.
- Staffend, N. A., Loftus, C. M., & Meisel, R. L. (2011). Estradiol reduces dendritic spine density in the ventral striatum of female Syrian hamsters. *Brain Structure and Function*, *215*, 187–194.
- Westwood, F. R. (2008). The female rat reproductive cycle: A practical histological guide to staging. *Toxicologic Pathology*, *36*, 375–384.
- Willett, J. A., Cao, J., Johnson, A., Patel, O. H., Dorris, D. M., & Meitzen, J. (2020). The estrous cycle modulates rat caudate-putamen medium spiny neuron physiology. *European Journal of Neuroscience*, *52*, 2737–2755.
- Willett, J. A., Will, T., Hauser, C. A., Dorris, D. M., Cao, J., & Meitzen, J. (2016). No evidence for sex differences in the electrophysiological properties and excitatory synaptic input onto nucleus accumbens shell medium spiny neurons. *eNeuro*, *3*, ENEURO.0147–15.2016.
- Wissman, A. M., May, R. M., & Woolley, C. S. (2012). Ultrastructural analysis of sex differences in nucleus accumbens synaptic connectivity. *Brain Structure and Function*, *217*, 181–190.
- Wissman, A. M., McCollum, A. F., Huang, G.-Z., Nikrodhanond, A. A., & Woolley, C. S. (2011). Sex differences and effects of cocaine on excitatory synapses in the nucleus accumbens. *Neuropharmacology*, *61*, 217–227.
- Woolley, C., Gould, E., Frankfurt, M., & McEwen, B. (1990). Naturally occurring fluctuation in dendritic spine density on adult hippocampal pyramidal neurons. *Journal of Neuroscience*, *10*, 4035–4039.
- Woolley, C. S., & McEwen, B. S. (1993). Roles of estradiol and progesterone in regulation of hippocampal dendritic spine density during the estrous cycle in the rat. *Journal of Comparative Neurology*, *336*, 293–306.
- Woolley, C. S., Weiland, N. G., McEwen, B. S., & Schwartzkroin, P. A. (1997). Estradiol increases the sensitivity of hippocampal CA1 pyramidal cells

- to NMDA receptor-mediated synaptic input: Correlation with dendritic spine density. *Journal of Neuroscience*, 17, 1848–1859.
- Xiao, L., & Becker, J. B. (1994). Quantitative microdialysis determination of extracellular striatal dopamine concentration in male and female rats: Effects of estrous cycle and gonadectomy. *Neuroscience Letters*, 180, 155–158.
- Yost, K. E., Quigley, J. A., & Becker, J. B. (2018). Rapid effects of ovarian hormones in dorsal striatum and nucleus accumbens. *Hormones and Behavior*, 104, 119–129.

How to cite this article: Beeson, A. L. S., & Meitzen, J. (2023). Estrous cycle impacts on dendritic spine plasticity in rat nucleus accumbens core and shell and caudate–putamen. *Journal of Comparative Neurology*, 531, 759–774. <https://doi.org/10.1002/cne.25460>